A computational fluid dynamics and finite element analysis design of a microtubular solid oxide fuel cell stack for fixed wing mini unmanned aerial vehicles

B. Hari[1], J. P. Brouwer[2], A. Dhir[1], R. Steinberger-Wilckens[1*]
[1]University of Birmingham, School of Chemical Engineering,
Edgbaston, B15 2TT Birmingham, United Kingdom
[2]HyGear Fuel Cell Systems B.V.,
P.O. Box 5280, 6802 EG Arnhem, The Netherlands

Abstract

Computational fluid dynamics (CFD) and finite element analysis (FEA) are important modelling and simulation techniques to design and develop fuel cell stacks and their balance of plant (BoP) systems.
The aim of this work is to design a microtubular solid oxide fuel cell (SOFC) stack by coupling CFD and FEA models to capture the multiphysics nature of the system. The focus is to study the distribution of fluids inside the fuel cell stack, the dissipation of heat from the fuel cell bundle, and any deformation of the fuel cells and the stack canister due to thermal stresses, which is important to address during the design process. The stack is part of an innovative all-in-one SOFC generator with an integrated BoP system to power a fixed wing mini unmanned aerial vehicle. Including the computational optimisation at an early stage of the development process is hence a prerequisite in developing a reliable and robust all-in-one SOFC generator system. The presented computational model considers the bundle of fuel cells as the heat source. This could be improved in the future by replacing the heat source with electrochemical reactions to accurately predict the influence of heat on the stack design.

Keywords: Computational fluid dynamics, fuel cell stack and system design, hydrocarbon fuel, microtubular solid oxide fuel cell, power supply, unmanned aerial vehicle

1. Introduction

Unmanned aerial vehicles (UAVs) have a limited range and time spent in the air. In the past, they were mainly used for military purposes. Today, they are rapidly expanding into new areas for civilian applications such as surveillance of public events, aerial photography, monitoring animal migrations and agricultural activities, mapping land, wildfire monitoring, and others. UAVs are traditionally powered by internal combustion engines and gas turbines. Such power systems are not the most appropriate for mini UAVs, which demand lighter power systems and quiet operation with similar flight duration as their conventional counterparts. Batteries and fuel cells offer an attractive alternative. The current state-of-the-art lithium-ion batteries for mini UAVs are heavy, require long charging times and cannot assure extended flight missions. Polymer electrolyte fuel cells (PEFCs) [1] or the combination of fuel cell and rechargeable battery [2] as a hybrid power system offer an alternative solution. Apart from hydrogen compressed in gas cylinders as the only possible fuel for PEFCs, other liquid fuels are gaining in popularity. Some reports suggest using sodium borohydride as the fuel for PEFCs [3] or propane as the fuel for microtubular solid oxide fuel cells (SOFCs) [4,5] to power mini UAVs. The use of conventional hydrocarbon fuels in a liquid form reduces the volume of the tank, avoids its pressurisation, and does not require any novel fuel supply infrastructure.
An SOFC stack directly converts chemical energy of hydrogen or hydrocarbon fuels into electricity and heat with a high electrical efficiency. Water (H_2O) and carbon dioxide (CO_2) are the only

*Corresponding author.
E-mail addresses: b.hari@bham.ac.uk (B. Hari), jan.peter.brouwer@hygear.nl (J. P. Brouwer), a.dhir@bham.ac.uk (A. Dhir), r.steinbergerwilckens@bham.ac.uk (R. Steinberger-Wilckens)

reaction products. Several types of SOFC stacks have been developed to date such as quadrilateral planar [6], all ceramic quadrilateral planar [7], circular planar [8,9], tubular [10], microtubular [11–14], cone shaped segmented-in-series tubular [15], segment-in-series tubular [16], segmented-in-series flattened tubular [17–19], flattened tubular [20,21], honeycomb [22,23], and micro [24] designs. Microtubular SOFC stacks are quite rare in applications compared to planar SOFC stacks. But they are easier to assemble since they require fewer assembly components. The main challenge for microtubular SOFCs remains connecting the electrode current collectors with the fuel cell electrodes [25–27], and preventing the stack from fuel and oxidant leakage [28–30]. These microtubular types of stacks have several advantages over planar counterparts, especially for dynamic applications such as UAVs. Small microtubular SOFC stack sizes allow faster start-up times with a good thermal shock resistance, improved cycling performance and simpler manufacturing [31] as long as their geometric dimensions are small enough to deliver high thermo-mechanical robustness.

1.1. State-of-the-art in computational modelling

Published papers mostly focus on using computational fluid dynamics (CFD) models for planar SOFC stacks and systems to analyse and optimise fuel and oxidant flows, temperature distribution, and concentration of products inside the interconnector plates, entire stacks or balance of plant (BoP) systems. One of the early publications, using the CFD software ANSYS Fluent to complement a microtubular SOFC stack design to minimise temperature gradients and maximise the use of produced heat, was reported by Lockett et al. [32]. The SOFC stack was built of 20 microtubular SOFCs and tested in a furnace, whereas the CFD simulation was used to approximate temperature distribution on a single microtubular SOFC by varying hydrogen and air flow rates. The study found that too high temperature degrades a SOFC material and too low temperature impairs fuel cell power. Recently, Sun and Ni [33] developed a three-dimensional SOFC stack model with direct internal reforming of methane using the CFD and finite element analysis (FEA) software COMSOL Multiphysics to investigate effects of interconnect rib size, temperature distribution, concentration of products, and current density distribution on the stack design. The study suggested that the Ra ratio of 0.3 for different combinations of methane and steam fuels, and the Ra ratio of 0.2 for hydrogen fuel are the optimum values for the best performance of the SOFC stack. On the other hand, coupled CFD and FEA models, which represent more realistic multiphysics computational models, are still rarely reported in scientific literature. The coupled models hence capture more detailed phenomena and thus better predict the behaviour of microtubular SOFCs during experiments. Such detailed multiphysics SOFC stack models can significantly reduce the development process in terms of time and costs. An extensive literature review of computational models with included case studies describing complex thermo-mechanical behaviour in SOFCs over the last decade was summarised by Peksen [34]. An early computational work on planar SOFC with coupled CFD and FEA models was reported by Selimovic et al. [35]. Coupled thermal and electrochemical models, developed in FORTRAN, were further combined with a thermal stress FEA model available in the CFD and FEA software FEMLAB. The authors investigated thermal stresses in the ceramic fuel cell due to differences in thermal expansion coefficients at high operating temperature using pre-reformed methane. The analysis showed that a modified gas flow arrangement can improve the fuel cell performance but might affects its ceramic structure. Hence, an addition of metallic interconnects improved the temperature distribution and lowered thermal stresses. Lin et al. [36] characterised thermal stresses in a planar SOFC stack made of three cells with a three-dimensional FEA thermo-electrochemical model during the start-up, steady-state and shut-down stages. The authors investigated cell positions, temperature gradients, viscosity of glass-ceramic sealant and thermal expansion mismatch between stack components. The simulation results suggested that the sealant is the most critical part of the assembly, whilst the metallic interconnect and the frame remained in the allowable range, depending on the accepted plastic deformation. Weil and Koeppel [37] used a thin deformable metal foil, known as the bonded compliant seal, to hermetically seal the fuel cell and its frame components in planar SOFC stacks. They used ANSYS 8.0 software to carry out three-dimensional FEA modelling for thermally induced stresses and strains within the seal during the heating and cooling conditions. The computational study found that the cell bowing increased up to 2.4 mm when the cell structure was cooled down to room temperature and the initial seal

design thus required further modification. The thermal stresses that developed within the structure were transferred to the sealing foil and absorbed as elastic and plastic strain. The thermal stresses decreased during the computationally induced second thermal cycle. Chiang et al. [38] evaluated fuel and oxidant gas distributions and thermal stresses in an anode supported SOFC under various conditions with a complex software setup. The aim of this study was to validate experimental results with computational ones. The authors used the CFD software Star-CD to simulate flow and temperature distributions with electrochemical reactions in the single cell and current-voltage characteristics. The temperature field was then passed to the FEA software MARC for thermal stress analysis inside the single SOFC. Finally, a structural analysis of the SOFC was performed by the FEA software PATRAN. The study concluded a good agreement of computational and experimental results. Fischer and Seume [39] developed a finite element mechanical model of a tubular SOFC with COMSOL Multiphysics. They coupled this model with a two-dimensional thermo-electrochemical model developed in MATLAB to provide realistic temperature profiles for the mechanical model. Finally, the authors then analysed the impact of methane internal reforming on thermo-mechanical stress and its distribution inside the SOFC at different temperatures. The simulation results showed strong dependence of the stress distribution and its magnitude on the methane reforming. Serincan et al. [40] developed a two-dimensional CFD model and analysed the effects of operating conditions on the microtubular SOFC performance such as flow rate, fuel composition, temperature and electrodes pressure with COMSOL Multiphysics. The study revealed that a high temperature increased the fuel cell performance due to increased catalytic activity and ionic conductivity and decreased mass transport loses. The internal current leaks through the electrolyte were also more significant at higher operating temperatures. Serincan et al. [41] further extended the previous study with the FEA analysis to investigate thermal stresses in the microtubular SOFC due to mismatch in thermal expansion coefficients between the fuel cell, sealant and alumina tube fuel cell holder during the experiment. The analysis found that the stresses in the sealant at the interface between the fuel cell and its holder changed significantly whereas the effect of temperature gradients on the stress distribution was almost negligible at mid-range current densities. Blum et al. [42] also investigated the effect of hermetic glass ceramic sealing on the planar SOFC stack during thermal cycling in combination with the test on a dummy planar SOFC stack and computational FEA modelling. The use of FEA gave the study a comprehensive understanding of the sealing behaviour under various parameters and what conditions caused cracks in the sealing material. A further analysis needs to be done to develop glass materials with improved material strength. Peksen et al. [43] presented a coupled three-dimensional thermo-fluid (CFD) and thermo-mechanical (FEA) model of a plate air pre-heater as part of a planar SOFC stack system. The temperature measurements of wall surfaces and gases were in good agreement with the computationally predicted models. The findings suggested that the coupled CFD and FEA models can be used to further optimise the air pre-heater. Further analysis revealed that thermo-mechanically induced stresses in the steel plates were caused by high temperature. The authors concluded that such a virtual analysis can reduce the product development time and costs, and optimise the pre-heater design prior to the prototype development process. Another study by Peksen [44] demonstrated a coupled three-dimensional thermo-fluid (CFD) and thermo-mechanical (FEA) analysis of a planar SOFC stack consisting of 36 cells. The analysis considered stack components such as a cell, wire mesh, frame, interconnector plate, and glass-ceramic sealants together with stack channels. The study gave a thorough insight of the fluid flow and temperature distribution across the stack assembly, and thermo-mechanically induced stresses in the steel components and sealants. In a similar study, Peksen et al. [45] introduced a three-dimensional thermo-mechanical analysis of a full scale planar SOFC short stack by coupling computational fluid dynamics and computational solid mechanics analyses. The authors considered an elasto-plastic behaviour of a cell component, a wire mesh, a metal frame, interconnector plates, and sealant materials as a function of temperature. The computational analysis of a transient thermal behaviour inside the stack predicted thermodynamically induced stresses during the heat-up, operation, and shut-down stages. It was found that the occurring stresses during the heat-up stage were the most critical of all operating stages and high strain in a sealant material lead to high deformation. Finally, Peksen [46] presented a three-dimensional multiphysics model of a complete planar SOFC system in this study by integrating CFD and FEA models and validated coupled simulation results against experimental data. The simulation model included a planar SOFC stack, air pre-heater, pre-reformer, afterburner, and auxiliary components.

It enabled visualisation of the whole system by predicting the fluid flow, temperature, and stress-strain distributions. The study revealed that the baffle and the heating plates have an important influence on the stack performance and needed to be redesigned. It was also suggested to use additional heating plates to mitigate thermal gradients of the fuel cell component. Finally, the use of a different steel material that was more resistant against strain due to high stresses in the components was highly recommended. Nakajo et al. [47] introduced a computational study of SOFC stacks with the FEA software ABAQUS that combined a thermo-electrochemical model with degradation effects and a thermo-mechanical model. Such a coupled modelling framework could address the effects of operating conditions on stresses in electrodes that contribute to the probability of their failure. The study concluded that the anode failure depended on temperature profiles, whereas the cathode failure depended on the thermal expansion mismatch with other fuel cell layers. Adjusting the flow, temperature, system specific power, and the fuel conversion fraction can reduce the probability of electrode failure by factors of 30 to 300. On the other hand, gadolinium-doped ceria mechanical properties and metallic interconnect thickness can reduce such probability in the range of 0.85 to 1.23. The authors suggested that further research was needed to understand the correlation between mechanical reliability and electrochemical performance of the SOFC stacks. Another paper by Nakajo et al. [48] extended the previous study with modelling of electrochemical degradation during long-term operation and thermal cycling. This study concluded that the electrochemical degradation changes the temperature profile and thus exposed the fuel cell to failure. Deformations of the stack components caused contact pressure losses during thermal cycling and the risk of electrodes cracking. Choudhary [49] simulated an anode supported planar SOFC with methane internal reforming for co-flow and counter-flow configurations. This three-dimensional and combined thermo-fluid (CFD) and thermo-mechanical (FEA) model was developed with COMSOL Multiphysics. It investigated the impact of operating pressure, the effect of recirculation ratio on carbon deposition, and the air ratio on temperature and stress profiles due to electrochemical reactions during the start-up, heat-up and load change phases. The counter flow configuration yielded 8.23 % higher current density, but the co-flow configuration shown 22.58 % higher efficiency. Kong et al. [50] developed a two-dimensional axisymmetric microtubular SOFC model to study the influence of electrode thickness on residual stresses inside the fuel cell at room temperature. The results predicted that the anode was exposed to tension stress whereas the electrolyte and the cathode were exposed to compressive stress. The authors suggested that the stresses could be reduced by increasing the thickness of electrodes.

An early version of a microtubular SOFC stack model described in this study was presented by Pianko-Oprych et al. [51]. The CFD and FEA microtubular SOFC stack model was designed by coupling ANSYS Fluent, ANSYS Mechanical, and COMSOL Multiphysics software. This model was based on the first microtubular SOFC stack design published by Hari et al. [52] and later on upgraded by a more practical design appropriate for manufacturing [53, 54]. A group of our project partners developed a fuselage prototype for a mini UAV to integrate it with a commercially available microtubular SOFC generator from Ultra Electronics. The study presented by Giacoppo et al. [55] used ANSYS Fluent to simulate the temperature and airflow around the SOFC generator inside the fuselage. The authors concluded that the selected commercial SOFC generator was able to work properly in the confined fuselage space.

CFD software ANSYS Fluent was used in a recent study to design external manifolds in order to optimise flow distributions of fuel and air with included pressure variations for a 40 cell planar SOFC stack [56]. Due to the simplification of the computational model, electrochemical reactions, heat transfer, and mass transfer phenomena were ignored. The simulation results suggested that the flow distribution depended on the manifold geometry and number of inlet and outlet tubes. The results also summarised the importance of such design on the stack performance. The latest development in designing a full scale planar SOFC stack, as an addition to a three-dimensional computational multiphysics model, included optimising the heating-up time of the SOFC system. In such a study, three different design configurations of electrically heated plates were investigated on the heating-up performance [57]. An important factor to accurately predict performance and lifetime of SOFC stacks is to couple multiphysics models with degradation effects. A detailed three-dimensional electrochemical model with included momentum, mass and heat transfer equations was applied to a single planar SOFC and compared with experimental results [58]. The leading conditions causing degradation, such as overpotentials, partial pressures of reactants, and

temperature gradients were thoroughly investigated in this study.

2. All-in-one solid oxide fuel cell generator system and design

2.1. All-in-one solid oxide fuel cell generator system

Fig. 1 shows the basic flow diagram of the overall fuel cell system, indicating the all-in-one SOFC generator system boundaries with the internal and external BoP system components. Such a system is proposed to minimise the size of the burner and the heat exchanger. The ambient air is not directly fed into the cathode side of the microtubular SOFC stack. Since it is preheated in the heat exchanger and the burner, the all-in-one SOFC generator could be more compact than alternative designs. It hence fits into the tightly restricted fuselage of the UAV.
The all-in-one SOFC generator system uses propane as the fuel because of its high energy density of 46360 kJ kg^{-1}. Propane is liquid at low pressures between $3 \cdot 10^5$ Pa and $12 \cdot 10^5$ Pa, and ambient temperatures. It could be therefore stored in a very compact and lightweight tank compared to a compressed gas such as hydrogen. The tank does not require a separate pump and an evaporator as a heavier fuel would need. Before feeding the fuel into the microtubular SOFC stack, propane has to be pre-reformed to allow a stable electrochemical conversion within the SOFC. Propane is fed through the control valve into the catalytic partial oxidation (CPOx) reformer, where it converts with the reformer air into a mixture of mainly hydrogen (H_2) and carbon monoxide (CO). The CPOx reformer consists of a number of wire meshes coated with a catalyst, together with additional baffles and a start-up heater. This provides a compact and lightweight BoP component that can be easily and quickly started up to an operating temperature. The reformate fuel enters the microtubular SOFC stack where H_2 and CO are electrochemically converted into water (H_2O) and carbon dioxide (CO_2) with simultaneous production of electric power and heat. The depleted reformate gas known as the anode off-gas leaves the microtubular SOFC stack and enters the catalytic burner, where the non-converted H_2 and CO mix with an excess of heated ambient air from the heat exchanger. Both gases react there with oxygen (O_2) from the hot ambient air to produce H_2O, CO_2, and heat. The blower supplies the ambient air to the CPOx reformer, the microtubular SOFC stack, and the burner. The reformer air represents only a small fraction of the total ambient air flow, which is drawn from the main ambient air stream through the control valve. The rest of the air is preheated in the heat exchanger, which enters the burner and leaves it mixed with the anode off-gas as the burner exhaust or flue gas at a temperature of about 700 °C. The burner flue gas still contains a substantial amount of O_2 and is supplied to the cathode side of the microtubular SOFC stack where it is used as the cathode air. Using the burner flue gas as the cathode air is an efficient way to preheat the ambient air. The cathode air serves not only to supply O_2, but also to remove the excess heat from the microtubular SOFC bundle. The heat removal largely determines the required cathode air flow rate. The cathode off-gas is then led into the heat exchanger to preheat the incoming ambient air from the blower and is vented through the exhaust into the atmosphere.

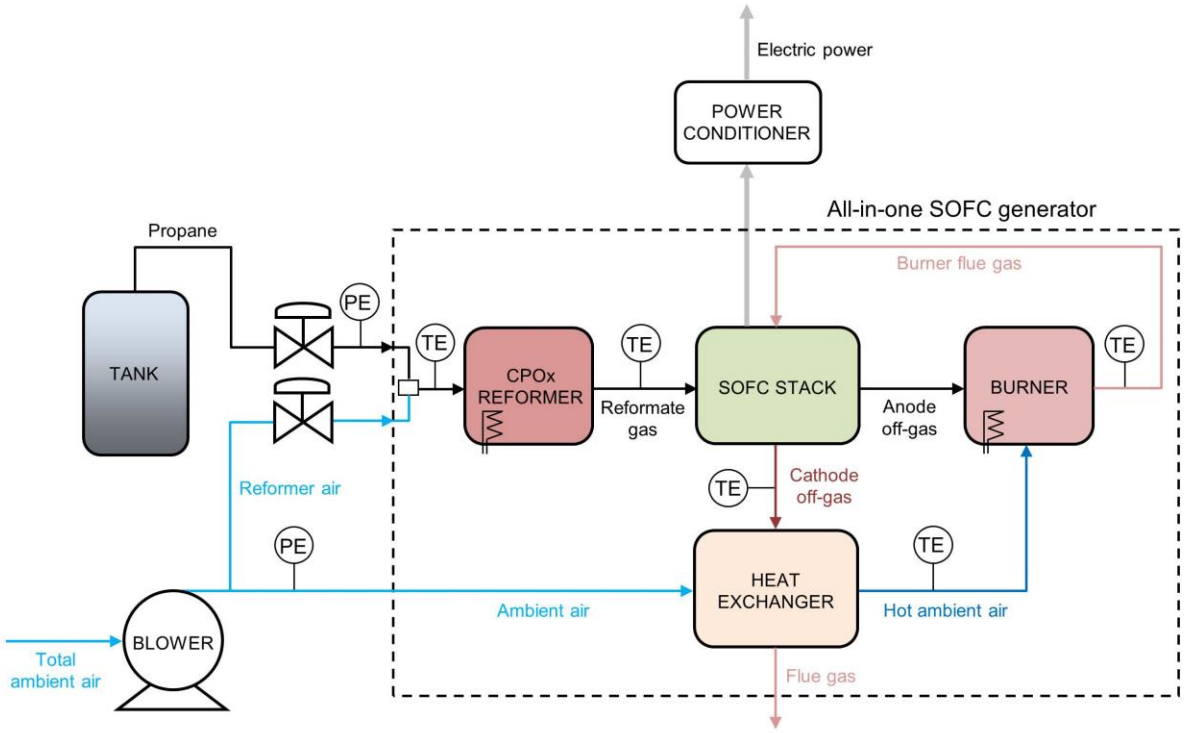

Fig. 1. All-in-one solid oxide fuel cell generator system with the balance of plant system components.

2.2. All-in-one solid oxide fuel cell generator design

The all-in-one SOFC generator system is constructed under strict geometric restrictions to fit into the UAV fuselage and at the same time to meet challenging weight limits. To meet these requirements, a cylindrical all-in-one SOFC generator is designed as shown in Fig. 2. Within the available constrained space, a compromised solution has to be found to achieve a high-quality mixing between propane and reformer air, and between the anode off-gas and the cathode air. The flow distribution of reactants over the CPOx reformer and burner catalysts has to be very homogeneous to achieve an efficient conversion and avoid local temperature hot spots. Similarly, the distribution of the cathode air through the microtubular SOFC bundle has to be homogeneous as well, to ensure sufficient heat transfer and thus avoid local high temperature gradients. This is challenging to achieve during the design process because of the pressure drop limits due to system efficiency demands of 20 % electrical efficiency as well as due to restrictions of the lightweight blower. Based on these restrictions, the all-in-one SOFC generator has an approximate dimension of 160 mm x 275 mm. It is capable to produce about 360 W of power in operating mode and approximately weights 4.30 kg. Further optimisation can reduce its weight to approximately 2.70 kg by using lighter materials.

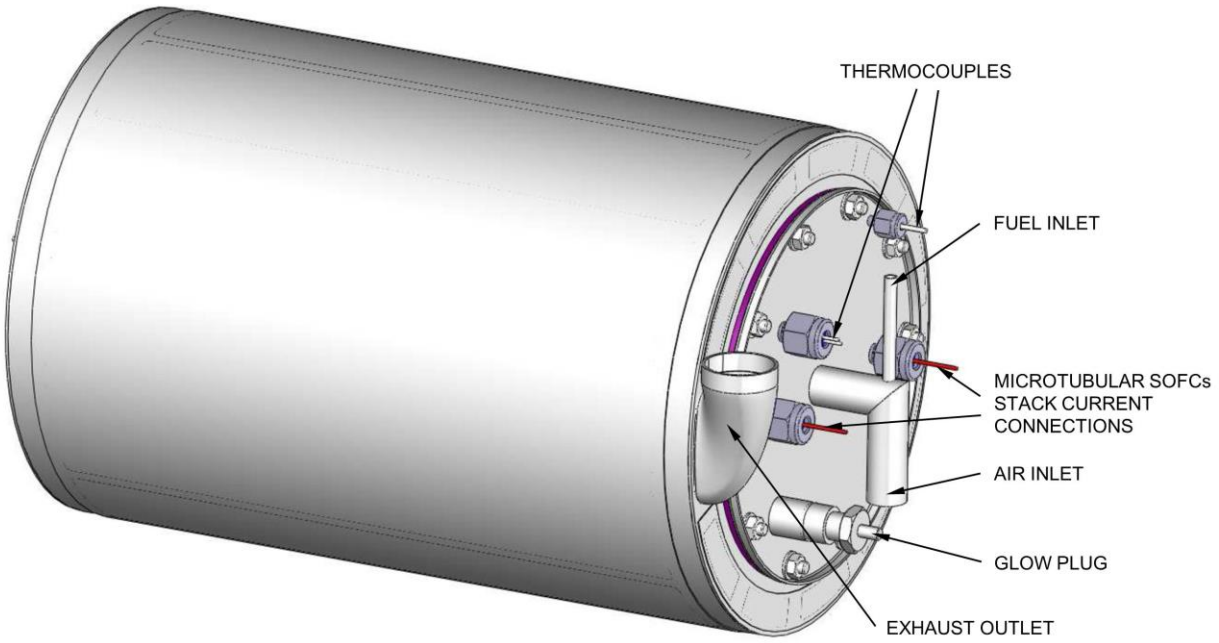

Fig. 2. All-in-one solid oxide fuel cell generator design.

3. Microtubular solid oxide fuel cell stack computational model

3.1. Computational geometry

Fig. 3 shows a three-dimensional half of the geometry of the microtubular SOFC stack divided into the fuel cell compartment and the dead zone. The fuel cell compartment of the full geometry consists of 48 microtubular SOFCs arranged into the bundle of three circular layers with 10, 16 and 22 fuel cells. The space between each neighbouring cell is about 5 mm wide, which is enough to supply the compartment with the cathode air and avoid short circuits between anode and cathode current collection points. The inlet and outlet manifolds are attached to both ends of the bundle to keep the fuel cells in place. They also prevent mixing the cathode air with the reformate fuel on the CPOx side and with the anode-off gas on the burner side.
The fuel enters the microtubular SOFC bundle from the inlet manifold and is subjected to electrochemical reactions inside the fuel cell anode channels. It leaves the fuel cell bundle as the depleted fuel, known as the anode off-gas, from the outlet manifold and enters into the dead zone. The dead zone is a short, 10 mm long compartment at the exhaust side of the bundle guiding the depleted fuel out of the stack. At the same time, it prevents a possible back flow of the depleted fuel from the burner into the fuel cell channels. On the other hand, the cathode air enters the fuel cell compartment through the central cathode air tube from the outlet manifold side. The air is then released out of the central cathode air tube through small holes perpendicular to the fuel cell bundle towards the outlet slits on the fuel cell canister. A number of small holes with different diameters on the central cathode air tube ensures an equal distribution of the cathode air flow through all three fuel cell layers along the bundle. This is important in order to minimise large temperature differences along each microtubular SOFC in the bundle, which might cause malfunction or even cracks on the fuel cell surface during operation. Several design configurations with different central cathode air tube lengths and diameters, with different number of holes and different canister slit dimensions were computationally investigated to achieve the most uniform cathode air distribution inside the fuel cell compartment.

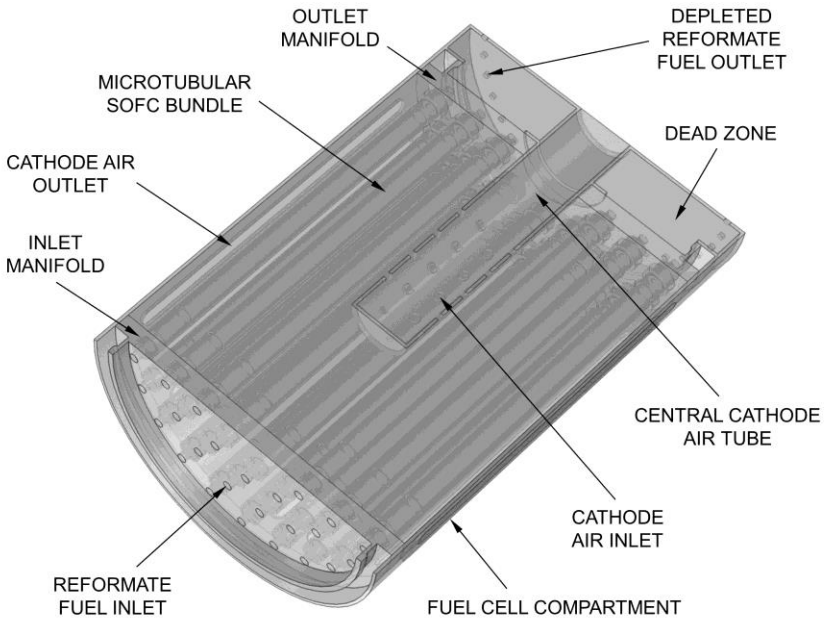

Fig. 3. 3D computational half-geometry of the microtubular solid oxide fuel cell stack.

Table 1 shows dimensions of the microtubular SOFC stack components as presented in Fig. 3.

Table 1
Microtubular solid oxide fuel cell stack components and design values.

Components	Design values
Diameter of microtubular SOFC stack	100.00 mm
Length of microtubular SOFC stack	132.10 mm
Length of microtubular SOFC compartment	122.10 mm
Diameter of central cathode air tube	18.00 mm
Length of central cathode air tube	70.00 mm
Number of holes on central cathode air tube	40
Diameter of holes on central cathode air tube	2.00 mm, 3.00 mm
Number of microtubular SOFC stack outlet slits	22
Length of microtubular SOFC stack outlet slits	110.00 mm
Width of microtubular SOFC stack outlet slits	5.00 mm
Number of microtubular SOFCs	48 (10, 16, 22)
Outer diameter of microtubular SOFCs	6.80 mm
Inner diameter of microtubular SOFCs	5.50 mm
Length of microtubular SOFCs	122.10 mm
Active length of microtubular SOFCs	95.30 mm
Length of dead zone	10 mm
Number of dead zone outlet holes	36
Diameter of dead zone outlet holes	2.00 mm

3.2. Computational mesh

Fig. 4 shows a three-dimensional half of the computational mesh of the microtubular SOFC stack designed by finite elements. The full mesh consists of the inlet and outlet manifolds, the bundle of 48 microtubular SOFCs, the canister with the central cathode air tube and the stack outlet slits, the fuel cell or cathode air compartment, and the dead zone. The computational mesh is modelled with COMSOL Multiphysics CFD and FEA software with 1638809 tetrahedral elements, 285665 triangular elements, 16358 edge elements and 1376 vertex elements. It is refined around the fuel

cells, the holes on the central cathode air tube, the outlet slits on the fuel cell canister and the holes on the dead zone to accurately capture transport phenomena of the entire computational model.

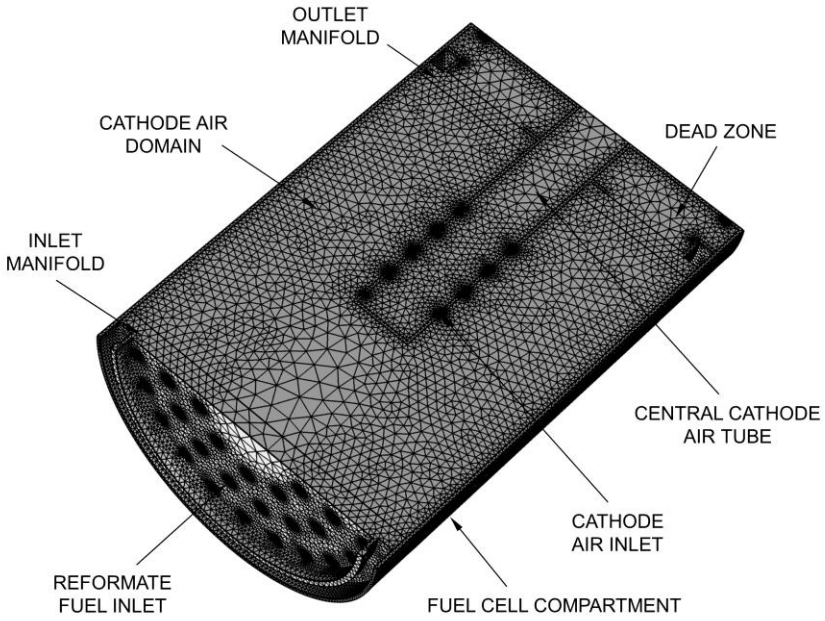

Fig. 4. 3D computational half-mesh of the microtubular solid oxide fuel cell stack.

3.3. Material properties

The microtubular SOFC stack includes the microtubular SOFC bundle with the inlet and outlet manifolds made of the ceramic material Macor. The stack is inserted into the canister with slits on the outer side, the perforated central cathode air tube, and the dead zone. Because of the high operating temperature between 650 °C and 750 °C, the canister material must withstand such harsh environment for long operating hours. Inconel X-750 steel is therefore chosen as the metal material. The entire microtubular SOFCs are set to be made of yttria stabilised zirconia ceramic material, without nickel catalyst particles, to simplify the computational model. For the same reason, the reformate fuel inside the fuel cell anode channels is assumed to have the properties of propane. The rest of the microtubular SOFC stack canister is filled with the cathode air to promote electrochemical reactions and to dissipate the heat produced by those reactions. Densities of propane and the cathode air are obtained from the ideal gas equation of state. Material properties are made temperature dependent by implementing polynomial approximations due to the high temperature. Dynamic viscosities, heat capacities at constant pressure and thermal conductivities of propane and the cathode air are calculated by polynomial equations.

Tables 2 to 4 show material properties of the microtubular SOFCs, the ceramic manifolds, and the microtubular SOFC stack canister from different manufactures used in this model such as Coorstek [59], Precision Ceramics [60], High Temp Metals [61], and Special Metals [62].

Table 2
Material properties of the microtubular solid oxide fuel cell from Coorstek.

Microtubular solid oxide fuel cell properties	Yttria stabilised zirconia
Density	6020 kg m^{-3}
Thermal conductivity	2.2 W m^{-1} K^{-1}
Heat capacity at constant pressure	400 J kg^{-1} K^{-1}
Coefficient of thermal expansion	$10.3 \cdot 10^{-6}$ K^{-1}
Young's modulus	$210 \cdot 10^{9}$ Pa

Poisson's ratio	0.23

Table 3
Material properties of the ceramic manifolds from Precision Ceramics.

Ceramic manifolds properties	Macor
Density	2520 kg m^{-3}
Thermal conductivity	1.46 W m^{-1} K^{-1}
Heat capacity at constant pressure	790 J kg^{-1} K^{-1}
Coefficient of thermal expansion	$12.6 \cdot 10^{-6}$ K^{-1}
Young's modulus	$66.9 \cdot 10^{9}$ Pa
Poisson's ratio	0.29

Table 4
Material properties of the microtubular solid oxide fuel cell canister from High Temp Metals and Special Metals.

Fuel cell canister properties	Inconel X-750
Density	8303 kg m^{-3}
Thermal conductivity	31.4 W m^{-1} K^{-1}
Heat capacity at constant pressure	526 J kg^{-1} K^{-1}
Coefficient of thermal expansion	$15.4 \cdot 10^{-6}$ K^{-1}
Young's modulus	$139.1 \cdot 10^{9}$ Pa
Poisson's ratio	0.29

3.4. Conservation and constitutive equations

The governing equations describing a thermo-fluid flow and the thermo-mechanical behaviour of the microtubular SOFC bundle with the supporting manifolds, the sealants, and the canister are described in this section. They consist of continuity, momentum and energy conservation equations together with thermo-elastic constitutive equations. Since the computational model is considered as a steady state model, time dependent terms are omitted from the equations. On the other hand, the computational model is simplified to avoid complex numerical calculations. Such a model also decreases the computational time due to the three-dimensional geometry and a large number of finite elements used to create a computational mesh. Hence, the CFD model is considered as a fluid flow and a heat transfer model without including species conservation equations and electrochemical reactions. These are modelled as a homogeneous heat source along the active surface area instead. The conservation and constitutive equations are discretised with the finite element method and solved as a multiphysics CFD and FEA model with COMSOL Multiphysics software.

3.4.1. Continuity and momentum conservation equations

The flow of reformate fuel inside the microtubular SOFCs and the flow of cathode air around the fuel cells is described by the continuity equation as:

$$\rho\left(\frac{\partial v_x}{\partial x}+\frac{\partial v_y}{\partial y}+\frac{\partial v_z}{\partial z}\right)=0 \tag{1}$$

and by the momentum equations in three-dimensional space as:

$$\rho\left(v_x\frac{\partial v_x}{\partial x}+v_y\frac{\partial v_x}{\partial y}+v_z\frac{\partial v_x}{\partial z}\right)=-\frac{\partial p}{\partial x}+\nu\,\rho\left(\frac{\partial^2 v_x}{\partial x^2}+\frac{\partial^2 v_x}{\partial y^2}+\frac{\partial^2 v_x}{\partial z^2}\right) \tag{2}$$

$$\rho\left(v_x\frac{\partial v_y}{\partial x}+v_y\frac{\partial v_y}{\partial y}+v_z\frac{\partial v_y}{\partial z}\right)=-\frac{\partial p}{\partial y}+\nu\,\rho\left(\frac{\partial^2 v_y}{\partial x^2}+\frac{\partial^2 v_y}{\partial y^2}+\frac{\partial^2 v_y}{\partial z^2}\right) \tag{3}$$

$$\rho\left(v_x\frac{\partial v_z}{\partial x}+v_y\frac{\partial v_z}{\partial y}+v_z\frac{\partial v_z}{\partial z}\right)=-\frac{\partial p}{\partial z}+\nu\,\rho\left(\frac{\partial^2 v_z}{\partial x^2}+\frac{\partial^2 v_z}{\partial y^2}+\frac{\partial^2 v_z}{\partial z^2}\right) \quad (4)$$

where $v_x\,[m\,s^{-1}]$, $v_y\,[m\,s^{-1}]$ and $v_z\,[m\,s^{-1}]$ are the velocity components of the reformate fuel and the cathode air, $\rho\,[kg\,m^{-3}]$ is the density of the reformate fuel and the cathode air, $\nu\,[m^2\,s^{-1}]$ is the kinematic viscosity of the reformate fuel and the cathode air, and $p\,[Pa]$ is the pressure.

3.4.2. Energy conservation equation

The reformate fuel and the cathode air inside the microtubular SOFC stack are exposed to an elevated operating temperature and are thus subject to convective heat transfer. The radiation term is neglected in this CFD model and predicted temperatures are therefore the highest possible. The heat transfer inside the microtubular SOFC stack is thus described by the energy equation as:

$$\rho\,c_p\left(v_x\frac{\partial T}{\partial x}+v_y\frac{\partial T}{\partial y}+v_z\frac{\partial T}{\partial z}\right)=k\left(\frac{\partial^2 T}{\partial x^2}+\frac{\partial^2 T}{\partial y^2}+\frac{\partial^2 T}{\partial z^2}\right)+\frac{P_{SOFC}}{V} \quad (5)$$

where $T\,[K]$ is the temperature of the reformate fuel and the cathode air, $k\,[W\,m^{-1}\,K^{-1}]$ is the thermal conductivity of the reformate fuel and the cathode air, $c_p\,[J\,kg^{-1}\,K^{-1}]$ is the specific heat capacity at constant pressure of the reformate fuel and the cathode air, $P_{SOFC}\,[W]$ is the thermal power generated by electrochemical reactions inside the microtubular SOFC bundle, and $V\,[m^3]$ is the volume of the microtubular SOFC bundle where electrochemical reactions take place.

3.4.3. Thermo-elastic constitutive equations

A high operating temperature between 650 °C and 750 °C in the microtubular SOFC stack canister induces mechanical and thermal stresses based on the Duhamel-Neumann Law. Such stresses cause deformations in the confined stack canister space measured by strains. It is assumed that the ceramic inlet and outlet manifolds, the cermet microtubular SOFC bundle, the ceramic sealants and the metal canister undergo isotropic linear elastic deformations during operation. These stack parts return to their original shapes when the stresses are removed. The total strain thus consists of the mechanical elastic strain and the thermal strain described as:

$$\varepsilon=\varepsilon_{M,el}+\varepsilon_T \quad (6)$$

The total strain can also be described with the normal stresses and the free thermal expansion coefficient due to the temperature difference as:

$$\varepsilon=\frac{\sigma}{E}+\alpha(T-T_0) \quad (7)$$

where $\varepsilon\,[-]$ is the total strain, $\varepsilon_{M,el}\,[-]$ is the mechanical elastic strain, $\varepsilon_T\,[-]$ is the thermal strain, $\sigma\,[N\,m^{-2}]$ is the normal stress, $E\,[N\,m^{-2}]$ is the modulus of elasticity or Young's modulus, $\alpha\,[K^{-1}]$ is the coefficient of linear thermal expansion, all in respect of the microtubular SOFC stack components, $T\,[K]$ is the temperature of the reformate fuel and the cathode air, assumed to be the same as the solid components of the SOFC stack, and $T_0\,[K]$ is the ambient temperature.

A total strain can be written in matrix form for a general three-dimensional object as:

$$\varepsilon=\begin{pmatrix}\varepsilon_{xx} & \varepsilon_{xy} & \varepsilon_{xz}\\ \varepsilon_{yx} & \varepsilon_{yy} & \varepsilon_{yz}\\ \varepsilon_{zx} & \varepsilon_{zy} & \varepsilon_{zz}\end{pmatrix} \quad (8)$$

with its three-dimensional components represented in terms of stresses as:

$$\varepsilon_{xx}=\frac{1}{E}\left(\sigma_{xx}-\nu\left(\sigma_{yy}+\sigma_{zz}\right)\right)+\alpha(T-T_0) \quad (9)$$

$$\varepsilon_{yy} = \frac{1}{E}\left(\sigma_{yy} - \nu(\sigma_{xx} + \sigma_{zz})\right) + \alpha(T - T_0) \quad (10)$$

$$\varepsilon_{zz} = \frac{1}{E}\left(\sigma_{zz} - \nu\left(\sigma_{xx} + \sigma_{yy}\right)\right) + \alpha(T - T_0) \quad (11)$$

$$2\varepsilon_{xy} = \frac{2(1+\nu)}{E}\sigma_{xy} \quad (12)$$

$$2\varepsilon_{xz} = \frac{2(1+\nu)}{E}\sigma_{xz} \quad (13)$$

$$2\varepsilon_{yz} = \frac{2(1+\nu)}{E}\sigma_{yz} \quad (14)$$

where $\varepsilon_{xx}\,[-]$, $\varepsilon_{yy}\,[-]$ and $\varepsilon_{zz}\,[-]$ are the normal strain components in x, y and z directions, $\varepsilon_{ij}\,[-]$ are the shear strain components in the j direction exerted on a plane perpendicular to the i axis, $\sigma_{xx}\,[\mathrm{N\,m^{-2}}]$, $\sigma_{yy}\,[\mathrm{N\,m^{-2}}]$ and $\sigma_{zz}\,[\mathrm{N\,m^{-2}}]$ are the normal stress components in x, y and z directions, $\sigma_{ij}\,[\mathrm{N\,m^{-2}}]$ are the shear stress components in the j direction exerted on a plane perpendicular to the i axis, and $\nu\,[-]$ is the Poisson's ratio, all in respect of the microtubular SOFC stack components.

The corresponding mechanical elastic and thermal stresses can be then expressed as the inverse relationship between the stresses and the strains in a three-dimensional space as:

$$\sigma = \begin{pmatrix} \sigma_{xx} & \sigma_{xy} & \sigma_{xz} \\ \sigma_{yx} & \sigma_{yy} & \sigma_{yz} \\ \sigma_{zx} & \sigma_{zy} & \sigma_{zz} \end{pmatrix} \quad (15)$$

$$\sigma_{xx} = \frac{E}{(1+\nu)(1-2\nu)}\left((1-\nu)\varepsilon_{xx} + \nu\left(\varepsilon_{yy} + \varepsilon_{zz}\right)\right) - \frac{E}{1-2\nu}\alpha\,(T - T_0) \quad (16)$$

$$\sigma_{yy} = \frac{E}{(1+\nu)(1-2\nu)}\left((1-\nu)\varepsilon_{yy} + \nu(\varepsilon_{xx} + \varepsilon_{zz})\right) - \frac{E}{1-2\nu}\alpha\,(T - T_0) \quad (17)$$

$$\sigma_{zz} = \frac{E}{(1+\nu)(1-2\nu)}\left((1-\nu)\,\varepsilon_{zz} + \nu\left(\varepsilon_{xx} + \varepsilon_{yy}\right)\right) - \frac{E}{1-2\nu}\alpha\,(T - T_0) \quad (18)$$

$$\sigma_{xy} = \frac{E}{(1+\nu)}\varepsilon_{xy} \quad (19)$$

$$\sigma_{xz} = \frac{E}{(1+\nu)}\varepsilon_{xz} \quad (20)$$

$$\sigma_{yz} = \frac{E}{(1+\nu)}\varepsilon_{yz} \quad (21)$$

3.5. Boundary conditions

3.5.1. Thermo-fluid boundary conditions

The reformate fuel enters the bundle of 48 microtubular SOFCs with the volumetric flow rate $Q_{fuel,a} = 26.62\,\mathrm{l\,min^{-1}}$ and the temperature $T_{fuel,a} = 700\,℃$. The bundle of microtubular SOFCs is exposed to electrochemical reactions where electrons are released due to reactions between oxygen (O_2) ions released from the cathode air and the reformate fuel. The electrochemical reactions generate heat, which must be removed from the fuel cell bundle. The cathode air has thus two important roles, to remove the heat from the bundle and to supply O_2 to the fuel cell cathode side for electrochemical reactions to take place. To simplify the microtubular SOFC computational stack model, the electrochemical reactions are represented as the heat source on the cathode side that uniformly produces $P_{SOFC} = 7.5\,\mathrm{W}$ of power per single microtubular SOFC. The cathode air enters the microtubular SOFC stack through the holes on the central cathode air

tube with the volumetric flow rate $\mathrm{Q_{air,c}} = 236.67\,\mathrm{l\,min^{-1}}$ and a temperature between $\mathrm{T_{air,c}} = 650\,℃$ and $\mathrm{T_{air,c}} = 750\,℃$. It leaves the stack through the long slits on the stack canister. Due to the additional heat produced by the electrochemical reactions, the cathode air leaves the stack canister at a higher temperature. The anode off-gas coming out from the fuel cells outlet side, still containing some unconverted hydrogen (H_2), carbon monoxide (CO), or methane (CH_4), enters the dead zone and then the burner.

3.5.2. Thermo-mechanical boundary conditions

The microtubular SOFC bundle is sealed onto the inlet manifold with a ceramic sealant to prevent leakage of the reformate fuel and mixing with the cathode air in the fuel cell compartment. The sealant is represented as a fixed constrained boundary condition. At the outlet side, the microtubular SOFC bundle is allowed to freely move inside the outlet manifold due to different thermal expansion between the materials of fuel cells and manifolds. If the fuel cell bundle is sealed onto both manifolds, thermal stresses would crack the fuel cells and cause malfunction of the entire stack system. A contact between the outlet manifold and the fuel cells is hence designed with a tight tolerance to prevent leakage and mixing the reformate fuel with the cathode air.

Table 5 shows thermo-fluid and thermo-mechanical boundary conditions applied on the microtubular SOFC stack.

Table 5
Boundary conditions applied to the microtubular solid oxide fuel cell stack.

Boundary conditions	Design values
Inlet volumetric flow rate of reformate fuel	$Q_{fuel,a}$ = 0.00045 $m^3\ s^{-1}$
Inlet temperature of reformate fuel	$T_{fuel,a}$ = 973 K
Inlet volumetric flow rate of cathode air	$Q_{air,c}$ = 0.00395 $m^3\ s^{-1}$
Inlet temperature of cathode air (two cases modelled)	$T_{air,c}$ = 923 K, $T_{air,c}$ = 1023 K
Heat source	P_{SOFC} = 7.5 W
Inlet manifold and fuel cells	x = 0

3.6. Solver

The discretised continuity, momentum, energy and thermo-elastic equations are solved sequentially with the COMSOL Multiphysics segregated solver until convergence for two different inlet temperatures as shown in Fig. 5. Each set of algebraic equations is solved with a different solver to assure converged solution. The continuity equation (pressure) and the momentum equations (velocity) are solved together with the iterative GMRES (Generalised Minimal RESidual method) solver for 650 °C and 750 °C known as the segregated step 1. The stress equation (displacement) is solved with the direct MUMPS (MUltifrontal Massively Parallel sparse direct Solver) solver for 650 °C and 750 °C known as the segregated step 2. And the energy equation (temperature) is again solved with the iterative GMRES solver for 650 °C and 750 °C known as the segregated step 3. Fig. 5 shows three convergence plots for each set of equations with a rapidly falling monotonic curve. The segregated step 1 represents the convergence plot for the pressure variable and the velocity variables solved from the continuity equation and momentum equations. The segregated step 2 represents the convergence plot for the displacement variables solved from the stress equation. Finally, the segregated step 3 represents the convergence plot for the temperature variable solved from the energy equation. The solutions converge between 40 and 55 iterations with a relative tolerance set up to 0.001 by default for different inlet temperatures.

a) b)

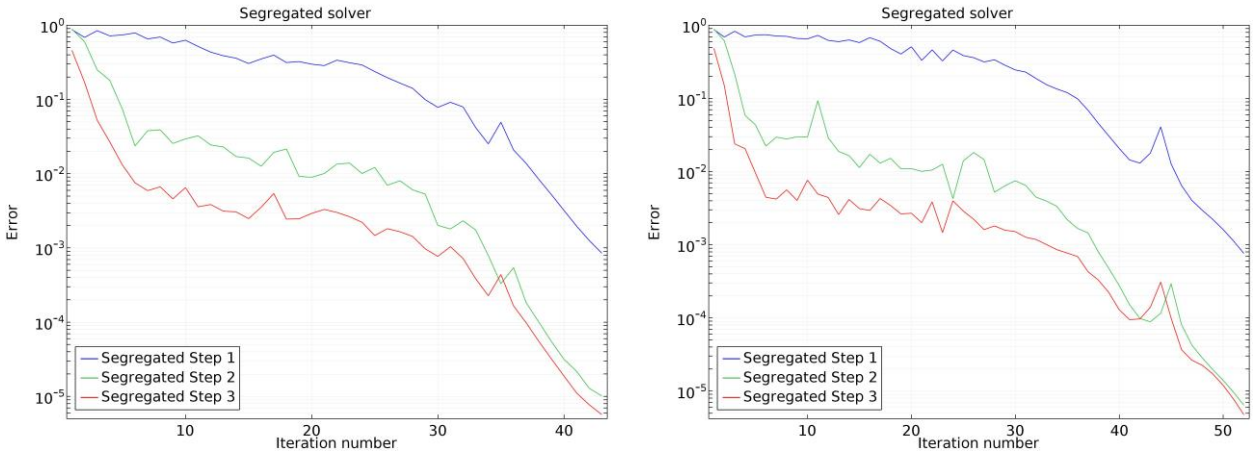

Fig. 5. Convergence plots at the cathode air inlet temperature of (a) 650 °C and (b) 750 °C.

4. Results and discussion

Several microtubular SOFC stack configurations were studied by varying the central cathode air tube length, its diameter with different number of holes and different canister slits dimensions. This section hence only presents results for the final microtubular SOFC stack CFD and FEA design.

Figs. 6 a and b show von Mises stresses applied on the microtubular SOFC stack during elastic deformation at the two different cathode air inlet temperatures 650 °C and 750 °C. Both figures show the stack canister with bent walls caused by elevated temperatures. The simulation results suggest that the 1 mm thin canister wall made of Inconel X-750 steel should be made thicker for the next prototype. High stresses inside the inlet manifold ring, compared to the rest of the stack, also indicate that this part of the stack must be carefully examined and possibly changed.

a)

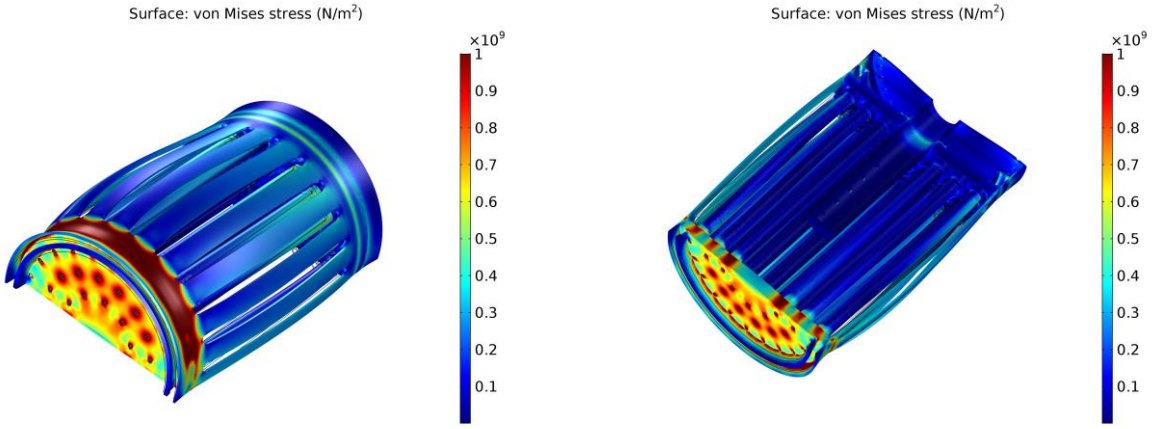

b)

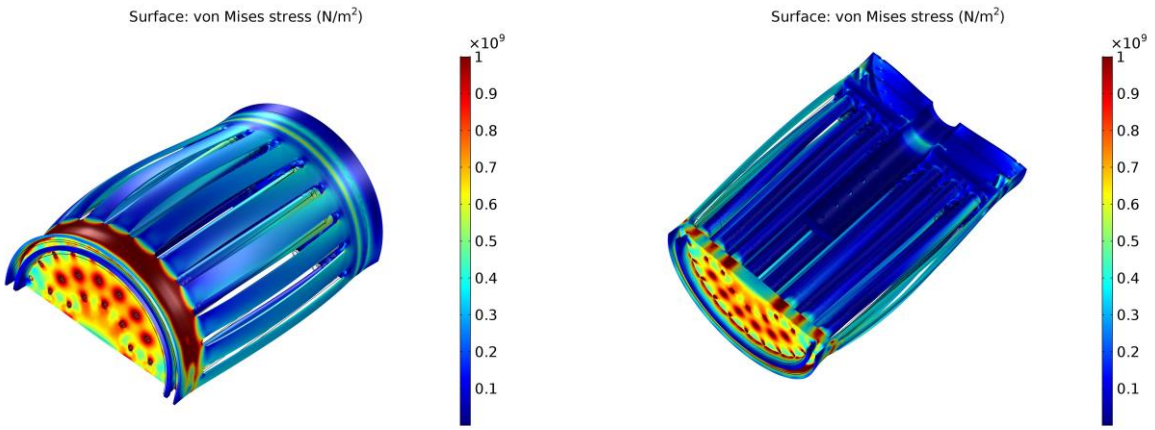

Fig. 6. Von Mises stresses distribution in the microtubular SOFC stack at the cathode air inlet temperature of (a) 650 °C and (b) 750 °C.

Figs. 7 a and b show the temperature distribution of the cathode air inside the microtubular SOFC stack and on the fuel cells at the two different cathode air inlet temperatures 650 °C and 750 °C. The simulation results suggest that the lowest temperature between 900 K and 1050 K is found on the inner fuel cell layer due to the direct contact with the cathode air bursting out of the holes on the central cathode air tube. As the cathode air penetrates towards the other two layers, it heats up and thus increases the temperature of the second layer. The highest temperature between 950 K and 1100 K with some hot spots is found on the outer layer of the fuel cell bundle where the cathode air escapes through the narrow gaps between the fuel cell layers into the canister slits. At cathode air inlet temperatures between 650 °C and 750 °C, the temperature difference along each fuel cell falls into the interval of 50 K. When the microtubular SOFC stack is thermally cycled with the temperature difference of about 50 K, thermal stresses might manifest into cracks on the fuel cells that ultimately lead to stack failure. Hence, the simulation results suggest that the microtubular SOFC stack should safely operate when the cathode air inlet temperature is at least 650 °C.

a)

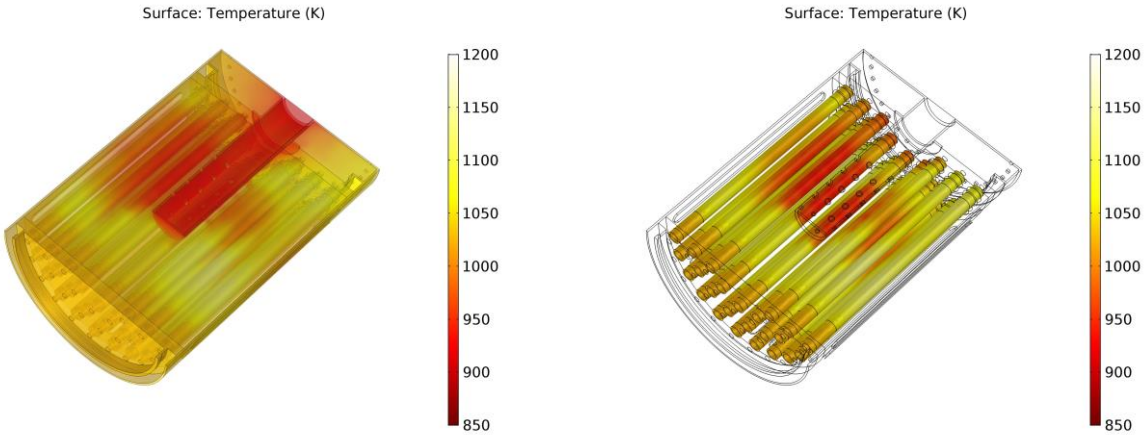

b)

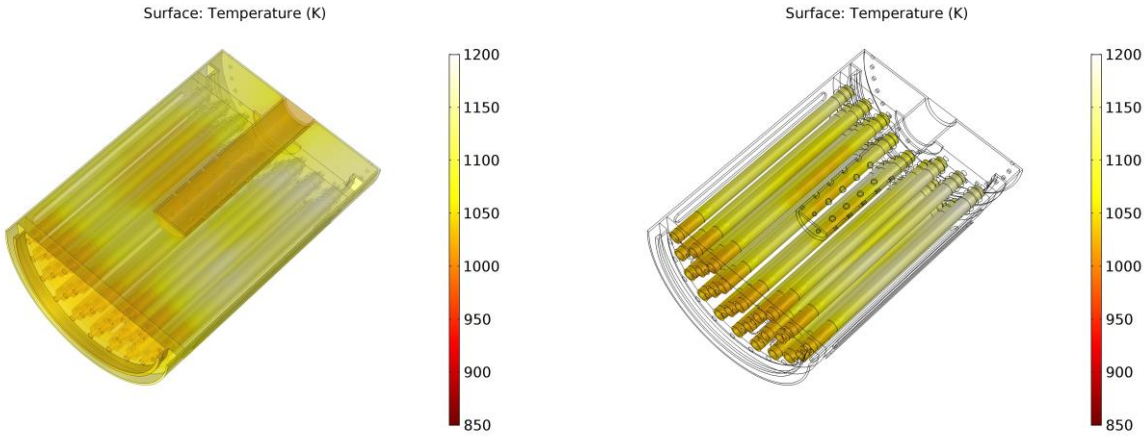

Fig. 7. Temperature distribution of the cathode air inside the microtubular SOFC stack and on the fuel cells at the cathode air inlet temperature of (a) 650 °C and (b) 750 °C.

Figs. 8 a and b show the velocity and streamlines distribution of the cathode air inside the microtubular SOFC stack at six different cross sections and at the two different cathode air inlet temperatures 650 °C and 750 °C. As expected, the simulation results suggest no difference in velocity magnitude and streamlines distribution when compared at different temperatures. This means that the temperature does not have a major effect on the flow pattern inside the stack. The highest velocities between 2.5 m s^{-1} and 5 m s^{-1} occur where the cathode air exits the central cathode air tube through the holes. The holes are evenly distributed along the central cathode air tube to ensure an equal distribution of the cathode air between the fuel cell layers. All of them get the same amount of the cathode air needed for electrochemical reactions to take place and for the transfer of heat from the fuel cell bundle through the canister slits. The simulation results of streamlines suggest a uniform distribution of the cathode air inside the microtubular SOFC stack achieved by carefully distributed holes on the central cathode air tube.

a)

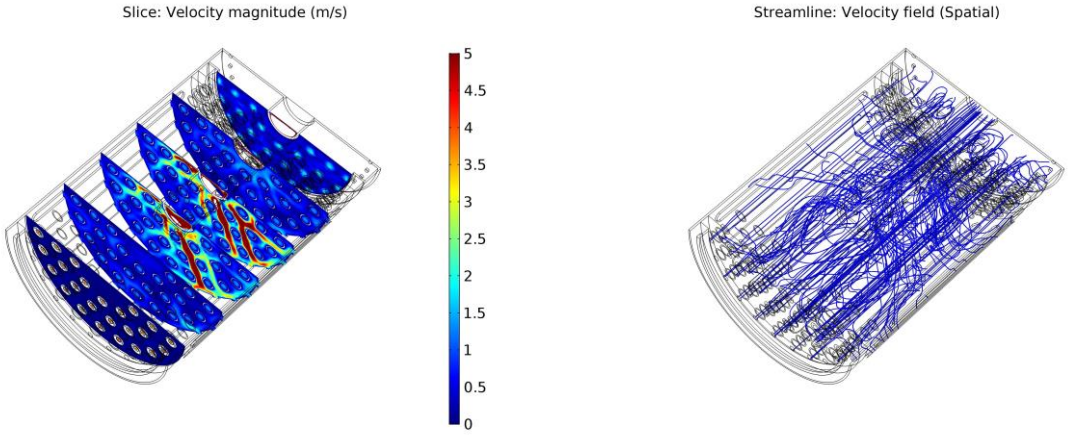

b)

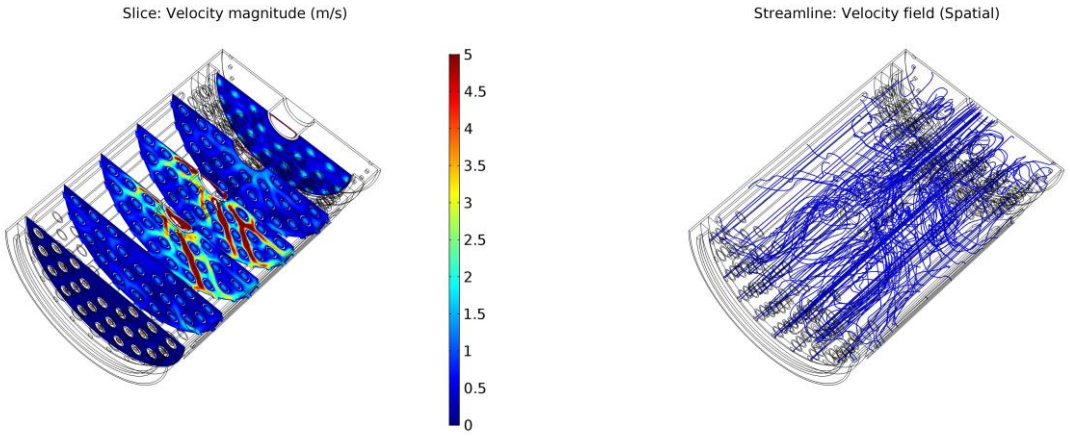

Fig. 8. Velocity and streamlines distribution of the cathode air inside the microtubular SOFC stack at the cathode air inlet temperature of (a) 650 °C and (b) 750 °C.

Figs. 9 a and b show the total displacement of the microtubular SOFC stack at the two different cathode air inlet temperatures 650 °C and 750 °C. The simulation results suggest no significant difference in the displacement of the fuel cell bundle and the canister when compared at different temperatures. The inlet side of the bundle would not expand due to the constraint since the fuel cells are sealed to the inlet manifold. On the other hand, the outlet side of the bundle would expand between 0.8 mm and 1.2 mm where fuel cells are allowed to freely move inside the outlet manifold. A part of the canister where the central cathode air tube is attached, would expand the most, between 1.4 mm and 1.8 mm when the temperature increases from 650 °C to 750 °C.

a) b)

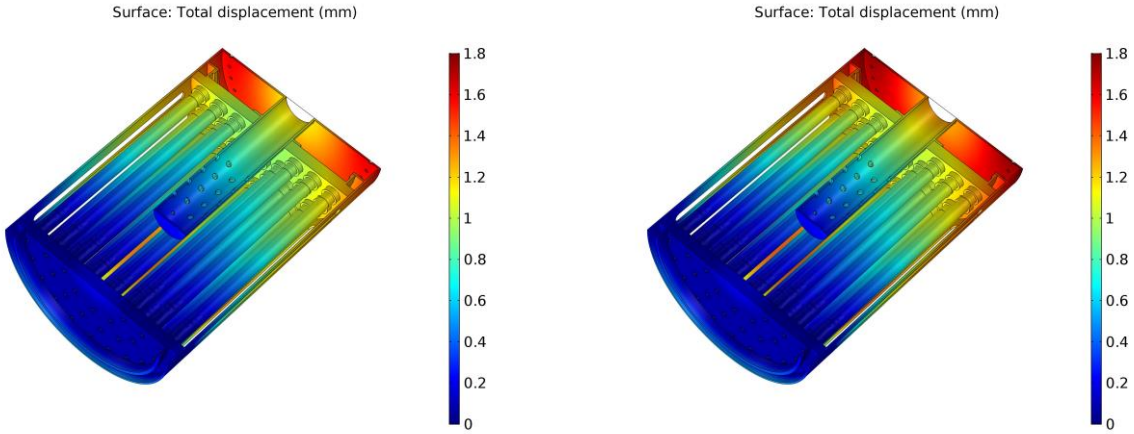

Fig. 9. Total displacement of the microtubular SOFC stack at the cathode air inlet temperature of (a) 650 °C and (b) 750 °C.

5. Conclusion

The novel microtubular SOFC stack has been designed with a CAD software and optimised with a CFD and FEA software. The computational modelling and simulation process has shown to be a very valuable technique in the preparation and optimisation stages to meet challenging design constraints. The simulation results suggest a temperature difference of about 150 K between the inner and the outer fuel cell layers. This difference could be reduced, if more space were allowed between the fuel cell layers for the cathode air to pass through and hence to cool the microtubular SOFC bundle. More space would increase the stack diameter and consequentially the size of the entire all-in-one SOFC generator. This is not possible with the current microtubular SOFC stack design because of the size restriction of the UAV fuselage design. An alternative solution would be

to use only two fuel cell layers with the existing diameter of the stack, but that might not produce enough power for the mini UAV to achieve the required flight time. Manufacturing longer microtubular SOFCs or cells with a larger diameter would be another solution. The hot cathode air inside the fuel cell compartment heats up the microtubular SOFC bundle and the stack canister, and deforms them due to prolonged exposure to the elevated temperature. In order to avoid high deformation caused by thermal stresses, the canister walls need to be thicker. The existing microtubular SOFC stack model could be extended with radiation effects to more accurately predict the temperature distribution inside the stack. Propane, as the reformate fuel, could be modelled as a mixture of nitrogen (N_2), carbon monoxide (CO), and hydrogen (H_2) with some content of water (H_2O) and methane (CH_4) as well. Furthermore, the next computational microtubular SOFC stack model has to be upgraded with the fuel and oxidant electrochemical reactions instead of assuming the cathode part of the microtubular SOFC bundle as a heat source. This could be achieved by modelling electrochemical reactions in one dimension and couple the generated heat with the active area of the three dimensional SOFC bundle model.
The designed all-in-one SOFC generator for mini UAVs is according to our knowledge the first compact microtubular SOFC system developed to date with a microtubular SOFC stack that can be replaced at the end of life. Such design simplifies the manufacturing process and reduces the overall production costs. The next step will be to test the microtubular SOFC stack prototype in the laboratory. These results will be then compared with the predicted computational results and new design improvements will be implemented on the all-in-one SOFC generator if needed until satisfactory results are achieved for commercial use.

Acknowledgements

The SOFC Unmanned Aerial Vehicle (SUAV) research project “Microtubular Solid Oxide Fuel Cell Power System Development and Integration into a Mini-UAV” was part-supported by the Fuel Cell and Hydrogen Joint Undertaking (Grant Agreement Number 278629). The information contained in this work reflects the views of the authors only. The authors gratefully acknowledge support from the SUAV partners: Adelan Ltd. (United Kingdom), Airbus Group Innovations (Germany), Airbus Group Innovations (United Kingdom), Catator AB (Sweden), CNR-ITAE (Italy), efceco (Germany), HyGear Fuel Cell Systems B.V. (The Netherlands), SURVEY Copter (France) and Zachodniopomorski Uniwersytet Technologiczny w Szczecinie (Poland).

References

[1] T. H. Bradley, B. A. Moffitt, D. N. Mavris, D.E. Parekh, Development and experimental characterization of a fuel cell powered aircraft, J. Power Sources 171 (2007) 793-801.
[2] T. Kim, S. Kwon, Design and development of a fuel cell-powered small unmanned aircraft, Int. J. Hydrogen Energy 37 (2012) 615-622.
[3] K. Kim, T. Kim, K. Lee, S. Kwon, Fuel cell system with sodium borohydride as hydrogen source for unmanned aerial vehicles, J. Power Sources 196 (2011) 9069-9075.
[4] A. D. Meadowcroft, S. Howroyd, K. Kendall, M. Kendall, Testing micro-tubular SOFCs in unmanned air vehicles (UAVs), ECS Trans. 57 (2013) 451-457.
[5] G. Giacoppo, O. Barbera, N. Briguglio, F. Cipitì, M. Ferraro, G. Brunaccini, E. Erdle, V. Antonucci, Thermal study of a SOFC system integration in a fuselage of a hybrid electric mini UAV, Int. J. Hydrogen Energy 42 (2017) 28022-28033.
[6] D. Penchini, G. Cinti, G. Discepoli, E. Sisani, U. Desideri, Characterization of a 100 W SOFC stack fed by carbon monoxide rich fuels, Int. J. Hydrogen Energy 38 (2013) 525-531.
[7] S. Giles, G. Lin, A. Mohanram, Y. Narendar, J. Pietras, F. C. Qi, W. R. Robbins, R. J. Sliwoski, Saint-Gobain’s all ceramic SOFC stack: architecture and performance, ECS Trans. 57 (2013) 105-114.
[8] K. Hayashi, M. Yokoo, Y. Yoshida, H. Arai, Solid oxide fuel cell stack with high electrical efficiency, NTT Technical Review 7 (2009) 1-5.
[9] A. Mai, B. Iwanschitz, U. Weissen, R. Denzler, D. Haberstock, V. Nerlich, A. Schuler, Status of Hexis’ SOFC stack development and the Galileo 1000 N micro-CHP system, ECS Trans.

35 (2011) 87-95.
[10] U. Mushtaq, S.-K. Kim, R.-H. Song, T.-H. Lim, J.-W. Lee, S.-B. Lee, S.-J. Park, Performance characteristics of 100 W carbon fuel cell stack based on SOFC technology, ECS Trans. 68 (2015) 2413-2419.
[11] N. M. Sammes, Y. Du, R. Bove, Design and fabrication of a 100 W anode supported micro-tubular SOFC stack, J. Power Sources 145 (2005) 428-434.
[12] T. Suzuki, Y. Funahashi, T. Yamaguchi, Y. Fujishiro, M. Awano, Cube-type micro SOFC stacks using sub-millimeter tubular SOFCs, J. Power Sources 183 (2008) 544-550.
[13] T. Suzuki, Y. Funahashi, T. Yamaguchi, Y. Fujishiro, M. Awano, New stack design of micro-tubular SOFCs for portable power sources, Fuel Cells 8 (2008) 381-384.
[14] V. Lawlor, S. Griesser, G. Buchinger, A. G. Olabi, S. Cordiner, D. Meissner, Review of the micro-tubular solid oxide fuel cell – Part I: Stack design issues and research activities, J. Power Sources 193 (2009) 387-399.
[15] J. Ding, J. Liu, A novel design and performance of cone-shaped tubular anode-supported segmented-in-series solid oxide fuel cell stack, J. Power Sources 193 (2009) 769-773.
[16] K. Miyamoto, M. Mihara, H. Oozawa, K. Hiwatashi, K. Tomida, M. Nishiura, H. Kishizawa, R. Mori, Y. Kobayashi, Recent progress of SOFC combined cycle system with segmented-in-series tubular type cell stack at MHPS, ECS Trans. 68 (2015) 51-58.
[17] Y. Matsuzaki, T. Hatae, S. Yamashita, Long-term stability of segmented type cell-stacks developed for residential use less than 1 kW, ECS Trans. 25 (2009) 159-166.
[18] K. Horiuchi, K. Nakamura, M. Matsuzaki, S. Yamashita, T. Horita, H. Kishimoto, K. Yamaji, H. Yokokawa, Durability tests of flatten tubular segmented-in-series type SOFC stacks for intermediate temperature operation, ECS Trans. 35 (2011) 217-223.
[19] H. Yoshida, T. Seyama, T. Sobue, S. Yamashita, Development of residential SOFC CHP system with flatten tubular segmented-in-series cells stack, ECS Trans. 35 (2011) 97-103.
[20] G. D. Agnew, R. D. Collins, M. Jorger, S. H. Pyke, R. P. Travis, The components of a Rolls-Royce 1 MW SOFC system, ECS Trans. 7 (2007) 105-111.
[21] T.-H. Lim, J.-L. Park, S.-B. Lee, S.-J. Park, R.-H. Song, D.-R. Shin, Fabrication and operation of a 1 kW class anode-supported flat tubular SOFC stack, Int. J. Hydrogen Energy 35 (2010) 9687-9692.
[22] M. Wetzko, A. Belzner, F. J. Rohr, F. Harbach, Solid oxide fuel cell stacks using extruded honeycomb type elements, J. Power Sources 83 (1999) 148-155.
[23] T. Yamaguchi, S. Shimizu, T. Suzuki, Y. Fujishiro, M. Awano, Fabrication and evaluation of a novel cathode-supported honeycomb SOFC stack, Mater. Lett. 63 (2009) 2577-2580.
[24] A. Bieberle-Hütter, D. Beckel, A. Infortuna, U. P. Muecke, J. L. M. Rupp, L. J. Gauckler, S. Rey-Mermet, P. Muralt, N. R. Bieri, N. Hotz, M. J. Stutz, D. Poulikakos, P. Heeb, P. Müller, A. Bernard, R. Gmür, T. Hocker, A micro-solid oxide fuel cell system as battery replacement, J. Power Sources 177 (2008) 123-130.
[25] A. Dhir, K. Kendall, Microtubular SOFC anode optimisation for direct use on methane, J. Power Sources 181 (2008) 297-303.
[26] Y. Funahashi, T. Shimamori, T. Suzuki, Y. Fujishiro, M. Awano, New fabrication technique for series-connected stack with micro tubular SOFCs, Fuel Cells 9 (2009) 711-716.
[27] V. Lawlor, K. Klein, C. Hochenauer, S. Griesser, S. Kuehn, A. G. Olabi, S. Cordiner, G. Buchinger, Experimental and numerical study of various MT-SOFC flow manifold techniques: Single MT-SOFC analysis, J. Fuel Cell Sci. Tech. 10 (2013) 011003-1-011003-11.
[28] P. A. Lessing, A review of sealing technologies applicable to solid oxide electrolysis cells, J. Mater. Sci. 42 (2007) 3465-3476.
[29] S. Hashimoto, H. Nishino, Y. Liu, K. Asano, M. Mori, Y. Funahashi, Y. Fujishiro, Development of evaluation technologies for microtubular SOFCs under pressurized conditions, J. Fuel Cell Sci. Tech. 5 (2008) 031208-1-031208-5.
[30] R. N. Singh, Self-repairable glass seals for solid oxide fuel cells, J. Mater. Res. 27 (2012) 2055-2061.
[31] K. Kendall, Progress in microtubular solid oxide fuel cells, Int. J. Appl. Ceram. Tec. 7 (2010) 1-9.
[32] M. Lockett, M. J. H. Simmons, K. Kendall, CFD to predict temperature profile for scale up of micro-tubular SOFC stacks, J. Power Sources 131 (2004) 243-246.
[33] Q. Sun, M. Ni, Three-dimensional modeling of internal reforming SOFC with a focus on the

interconnect size effect, ECS Trans. 68 (2015) 2317-2338.
[34] M. Peksen, Numerical thermomechanical modelling of solid oxide fuel cells, Prog. Energy Combust. Sci. 48 (2015) 1-20.
[35] A. Selimovic, M. Kemm, T. Torisson, M. Assadi, Steady state and transient thermal stress analysis in planar solid oxide fuel cells, J. Power Sources 145 (2005) 463-469.
[36] C.-K. Lin, T.-T. Chen, Y.-P. Chyou, L.-K. Chiang, Thermal stress analysis of a planar SOFC stack, J. Power Sources 164 (2007) 238-251.
[37] K. S. Weil, B. J. Koeppel, Thermal stress analysis of the planar SOFC bonded compliant seal design, Int. J. Hydrogen Energy 3 (2008) 3976-3990.
[38] L.-K. Chiang, H.-C. Liu, Y.-H. Shiu, C.-H. Lee, R.-Y. Lee, Thermo-electrochemical and thermal stress analysis for an anode-supported SOFC cell, Renewable Energy 33 (2008) 2580-2588.
[39] K. Fischer, J. R. Seume, Impact of the temperature profile on thermal stress in a tubular solid oxide fuel cell, J. Fuel Cell Sci. Techol. 6 (2009) 011017-1-011017-9.
[40] M. F. Serincan, U. Pasaogullari, N. M. Sammes, Effects of operating conditions on the performance of a micro-tubular solid oxide fuel cell (SOFC), J. Power Sources 192 (2009) 414-422.
[41] M. F. Serincan, U. Pasaogullari, N. M. Sammes, Thermal stresses in an operating micro-tubular solid oxide fuel cell, J. Power Sources 195 (2010) 4905-4914.
[42] L. Blum, S. M. Groß, J. Malzbender, U. Pabst, M. Peksen, R. Peters, I. C. Vinke, Investigation of solid oxide fuel cell sealing behavior under stack relevant conditions at Forschungszentrum Jülich, J. Power Sources 196 (2011) 7175-7181.
[43] M. Peksen, R. Peters, L. Blum, D. Stolten, 3D coupled CFD/FEM modelling and experimental validation of a planar type air pre-heater used in SOFC technology, Int. J. Hydrogen Energy 36 (2011) 6851-6861.
[44] M. Peksen, A coupled 3D thermofluid-thermomechanical analysis of a planar type production scale SOFC stack, Int. J. Hydrogen Energy 36 (2011) 11914-11928.
[45] M. Peksen, A. Al-Masri, L. Blum, D. Stolten, 3D transient thermomechanical behaviour of a full scale SOFC short stack, Int. J. Hydrogen Energy 38 (2013) 4099-4107.
[46] M. Peksen, 3D transient multiphysics modelling of a complete high temperature fuel cell system using coupled CFD and FEM, Int. J. Hydrogen Energy 39 (2014) 5137-5147.
[47] A. Nakajo, F. Mueller, J. Brouwer, J. Van herle, D. Favrat, Mechanical reliability and durability of SOFC stacks. Part I: Modelling of the effect of operating conditions and design alternatives on the reliability, Int. J. Hydrogen Energy 37 (2012) 9249-9268.
[48] A. Nakajo, F. Mueller, J. Brouwer, J. Van herle, D. Favrat, Mechanical reliability and durability of SOFC stacks. Part II: Modelling of mechanical failures during ageing and cycling, Int. J. Hydrogen Energy 37 (2012) 9269-9286.
[49] S. T. Choudhary, Computational analysis of IR-SOFC: Transient, thermal stress, carbon deposition and flow dependency, Int. J. Hydrogen Energy 41 (2016) 10212-10227.
[50] W. Kong, W. Zhang, S. Zhang, Q. Zhang, S. Su, Residual stress analysis of a micro-tubular solid oxide fuel cell, Int. J. Hydrogen Energy 41 (2016) 16173-16180.
[51] P. Pianko-Oprych, T. Zinko, Z. Jaworski, Simulation of thermal stresses for new designs of microtubular solid oxide fuel cell stack, Int. J. Hydrogen Energy 40 (2015) 14584-14595.
[52] B. Hari, J. P. Brouwer, A. Meadowcroft, A. Dhir, R. Steinberger-Wilckens, Computational modelling of a microtubular solid oxide fuel cell stack for unmanned aerial vehicles, 11th European SOFC and SOE Forum 2014, 1-4 July 2014, Lucerne, Switzerland.
[53] B. Hari, A. Dhir, R. Steinberger-Wilckens, A microtubular solid oxide fuel cell power system for a fixed wing mini unmanned aerial vehicle, FDFC 2015 – 6th International Conference on Fundamentals and Development of Fuel Cells, 3-5 February 2015, Toulouse, France.
[54] B. Hari, A. Dhir. R. Steinberger-Wilckens R, A thermo fluid and thermo mechanical modelling of a microtubular solid oxide fuel cell stack for unmanned aerial vehicles, ECS Trans. 68 (2015) 3133-3141.
[55] G. Giacoppo, O. Barbera, N. Briguglio, F. Cipitì, M. Ferraro, G. Brunaccini, E. Erdle, V. Antonucci, Thermal study of a SOFC system integration in a fuselage of a hybrid electric mini UAV, Int. J. Hydrogen Energy 42 (2017) 28022-28033.

[56] C. Zhao, J. Yang, T. Zhang, D. Yan, J. Pu, B. Chi, J. Li, Numerical simulation of flow distribution for external manifold design in solid oxide fuel cell stack, Int. J. Hydrogen Energy 42 (2017) 7003-7013.
[57] M. Peksen, Safe heating-up of a full scale SOFC system using 3D multiphysics modelling optimisation, Int. J. Hydrogen Energy 43 (2018) 354-362.
[58] M. Navasa, C. Graves, C. Chatzichristodoulou, T. L. Skafte, B. Sundén, H. L. Frandsen, A three dimensional multiphysics model of a solid oxide electrochemical cell: A tool for understanding degradation, Int. J. Hydrogen Energy 43 (2018) 11913-11931.
[59] http://www.coorstek.com/materials/ceramics/zirconia_YTZP_Sintered.php, retrieved in February 2016.
[60] http://www.precision-ceramics.co.uk/macor-machinable-glass-ceramic.htm, retrieved in February 2016.
[61] http://www.hightempmetals.com/techdata.php, retrieved in February 2016.
[62] http://www.specialmetals.com/assets/documents/alloys/inconel/inconel-alloy-x-750.pdf, retrieved in February 2016.